PHYSICAL REVIEW D **82,** 115031 (2010)

LHC phenomenology of a two-Higgs-doublet neutrino mass model

Shainen M. Davidson and Heather E. Logan*

Ottawa-Carleton Institute for Physics, Carleton University, Ottawa K1S 5B6 Canada

(Received 5 October 2010; published 30 December 2010)

We study the LHC search prospects for a model in which the neutrinos obtain Dirac masses from couplings to a second Higgs doublet with tiny vacuum expectation value. The model contains a charged Higgs boson that decays to $\ell\nu$ with branching fractions controlled by the neutrino masses and mixing angles as measured in neutrino oscillation experiments. The most promising signal is electroweak production of H^+H^- pairs with decays to $\ell\ell' p_T^{\rm miss}$, where $\ell\ell' = e^+e^-$, $\mu^+\mu^-$, and $e^\pm\mu^\mp$. We find that a cut on the kinematic variable M_{T2} eliminates most of the $t\bar{t}$ and W-pair background. Depending on the neutrino mass spectrum and mixing angles, a 100 (300) GeV charged Higgs could be discovered at the LHC with as little as 8 (24) fb^{-1} of integrated luminosity at 14 TeV pp center-of-mass energy.

DOI: 10.1103/PhysRevD.82.115031 PACS numbers: 14.80.Fd, 12.60.Fr, 14.60.Pq

I. INTRODUCTION

The standard model (SM) accounts for almost all experimental high energy physics data; however, the observation of neutrino oscillations requires that the SM be extended to include nonzero neutrino masses. While there are many ways to expand the SM to account for neutrino oscillations, we attempt to do so with the following goals. First, the neutrino mass scale is significantly lower than the mass scales of the other fermions, so we would like the model to account for this without the addition of many tiny parameters. Second, lepton number violation has not yet been observed, so we would like the model to give rise to Dirac neutrino masses, with Majorana masses forbidden. Third, we would like the model to be testable at the CERN Large Hadron Collider (LHC).

Most neutrino mass models give rise to Majorana masses for the SM neutrinos, with many predicting TeV-scale new physics accessible at the LHC. In contrast, only a few models for Dirac neutrinos have been proposed. These typically involve a second Higgs doublet with very small vacuum expectation value (vev) that couples only to the left-handed lepton doublets and the right-handed neutrinos, resulting in neutrino masses of the same order as the very small vev. The original SM-like Higgs doublet couples to all of the quarks and charged leptons in the usual way. Such a Yukawa coupling structure can be obtained by imposing a global Z_2 symmetry, as proposed in the models of Refs. [1,2]; however, this does not by itself forbid neutrino Majorana mass terms, which must instead be eliminated by imposing an additional lepton number symmetry. The required Yukawa coupling structure can also be obtained by imposing a global U(1) symmetry; this idea was first proposed in Ref. [3] as a way of ensuring the (then-assumed) masslessness of the neutrinos in the presence of right-handed neutrino states, and has the virtue of forbidding Majorana mass terms by itself.

In order to generate neutrino masses, the global symmetry used to ensure the desired Yukawa structure has to be broken. Spontaneous breaking leads to a very light scalar which can cause problems with standard big-bang nucleosynthesis [2], as well as having significant effects on the phenomenology of the new Higgs particles [4]. By instead breaking a global U(1) symmetry explicitly, the model proposed by us in Ref. [5] generates Dirac neutrino masses while avoiding very light scalars.[1] A supersymmetric version of this model was studied in Ref. [7], which found spectacular multilepton signals from cascade decays of the supersymmetric partners of the new Higgs bosons and right-handed neutrinos at the LHC.

In this paper we study the LHC detection prospects of the nonsupersymmetric model of Ref. [5]. This model expands the SM by adding a second Higgs doublet Φ_2 with the same electroweak quantum numbers as the SM Higgs doublet Φ_1, as well as adding three gauge-singlet right-handed Weyl spinors ν_{R_i} which will become the right-handed components of the three Dirac neutrinos. The model imposes a global U(1) symmetry under which the second Higgs doublet and the right-handed neutrinos have charge $+1$, while all the SM fields have charge zero. This allows Yukawa couplings of the second Higgs doublet only to the right-handed neutrinos and the SM lepton doublet, and forbids Majorana masses for the right-handed neutrinos. It also tightly constrains the form of the Higgs potential. Breaking the U(1) symmetry explicitly using a term $m_{12}^2\Phi_1^\dagger\Phi_2$ + H.c. in the Higgs potential yields a vev v_2 for the second Higgs doublet and consequently gives the neutrinos Dirac masses proportional to v_2. By requiring that $v_2 \sim \mathcal{O}(\text{eV})$, the Dirac neutrino masses are made suitably small without requiring tiny Yukawa couplings.

The characteristic feature of the model is that the couplings of the charged scalar pair $H^\pm$ and two neutral scalars

*logan@physics.carleton.ca

[1]A similar mechanism was used to explain the top-bottom quark mass hierarchy in Ref. [6].

H^0 and A^0 from the second Higgs doublet to leptons and neutrinos are controlled by the neutrino masses and mixing angles. In this paper we take advantage of the distinctive decay of the charged Higgs boson H^+ into charged leptons and neutrinos. We focus on electroweak pair production of H^+H^- at the LHC followed by decays to $\ell\ell' p_T^{\rm miss}$, where $\ell\ell'$ can be any combination of opposite-sign e, μ, and τ leptons and $p_T^{\rm miss}$ denotes missing transverse momentum (carried away by the neutrinos). Because τ leptons are more difficult to reconstruct experimentally, we concentrate on the final states with $\ell\ell' = e^+e^-$, $\mu^+\mu^-$, and $e^\pm\mu^\mp$. The major backgrounds are diboson production (W^+W^-, ZZ, and $Z\gamma$) and top quark pair production with both tops decaying leptonically.

To determine whether the H^+H^- signal will be detectable at the LHC, we generated signal and background events using MADGRAPH/MADEVENT version 4 [8] assuming 14 TeV pp center-of-mass energy. We present results both at parton level, and after hadronization with PYTHIA [9] and fast detector simulation with PGS [10]. With appropriate cuts, we find that a 5σ discovery can be achieved with luminosity in the range 8–75 fb^{-1} for $M_{H^+} = 100$ GeV, depending on the neutrino mixing parameters. For $M_{H^+} = 300$ GeV a 5σ discovery can be made with luminosity in the range 24–460 fb^{-1}. The higher luminosity requirements occur when the neutrino parameters are such that H^+ decays mostly to $\tau\nu$, leading to final states not considered in our analysis. We find that the kinematic variable M_{T2} is very effective at separating the signal from the $t\bar{t}$ and WW backgrounds for charged Higgs masses above the W mass, and also provides sensitivity to the charged Higgs mass.[2]

This paper is organized as follows. In the next section we review the model and present the charged Higgs decay branching ratios. In Sec. III we describe the signal and background processes, our event generation procedure and selection cuts, and the resulting signal significance. In Sec. IV we summarize our conclusions.

II. THE MODEL

As outlined in the introduction, we start with the field content of the SM and add to it a new scalar SU(2)$_L$ doublet Φ_2 (the SM Higgs is denoted Φ_1) and three right-handed gauge singlets ν_{R_i} (these are the right-handed neutrinos). We impose a U(1) symmetry under which Φ_2 and the three ν_{R_i} have charge $+1$ and all the other fields are uncharged, which leads to the Yukawa coupling structure [5]

$$\mathcal{L}_{\rm Yuk} = -y^d_{ij}\bar{d}_{R_i}\Phi_1^\dagger Q_{L_j} - y^u_{ij}\bar{u}_{R_i}\tilde{\Phi}_1^\dagger Q_{L_j} - y^\ell_{ij}\bar{e}_{R_i}\Phi_1^\dagger L_{L_j} - y^\nu_{ij}\bar{\nu}_{R_i}\tilde{\Phi}_2^\dagger L_{L_j} + \text{H.c.} \quad (1)$$

Here $\tilde{\Phi}_i \equiv i\sigma_2\Phi_i^*$ is the conjugate Higgs doublet and y^f_{ij} are the 3×3 Yukawa matrices for fermion species f.

The Higgs doublets can be written explicitly as

$$\Phi_i = \begin{pmatrix} \phi_i^+ \\ (v_i + \phi_i^{0,r} + i\phi_i^{0,i})/\sqrt{2} \end{pmatrix}, \quad (2)$$

where v_1 will be generated by the usual spontaneous symmetry breaking mechanism of the SM and v_2 will be generated by the explicit breaking of the global U(1), described below. Inserting these expressions for Φ_i into Eq. (1), we obtain the fermion masses and couplings to scalars. In particular, the fourth term in Eq. (1) gives rise to the neutrino mass matrix and interactions:

$$\mathcal{L}_{\rm Yuk} \supset -\frac{y^\nu_{ij}v_2}{\sqrt{2}}\bar{\nu}_{R_i}\nu_{L_j} - \frac{y^\nu_{ij}}{\sqrt{2}}\phi_2^{0,r}\bar{\nu}_{R_i}\nu_{L_j} - i\frac{y^\nu_{ij}}{\sqrt{2}}\phi_2^{0,i}\bar{\nu}_{R_i}\nu_{L_j} + y^\nu_{ij}\phi_2^+\bar{\nu}_{R_i}\ell_{L_j} + \text{H.c.} \quad (3)$$

After diagonalizing the mass matrix in the first term, the neutrino mass eigenvalues are given by $m_{\nu_i} = y^\nu_i v_2/\sqrt{2}$, where y^ν_i are the eigenvalues of y^ν_{ij}. In this way, the small masses of the three neutrinos can be traced to the small value of v_2.

We obtain the vevs of the scalar doublets from the Higgs potential as follows. The most general gauge-invariant scalar potential for two Higgs doublets is (see, e.g., Ref. [11]),

$$\begin{aligned} V = {} & m_{11}^2\Phi_1^\dagger\Phi_1 + m_{22}^2\Phi_2^\dagger\Phi_2 - [m_{12}^2\Phi_1^\dagger\Phi_2 + \text{H.c.}] \\ & + \frac{1}{2}\lambda_1(\Phi_1^\dagger\Phi_1)^2 + \frac{1}{2}\lambda_2(\Phi_2^\dagger\Phi_2)^2 \\ & + \lambda_3(\Phi_1^\dagger\Phi_1)(\Phi_2^\dagger\Phi_2) + \lambda_4(\Phi_1^\dagger\Phi_2)(\Phi_2^\dagger\Phi_1) \\ & + \left\{\frac{1}{2}\lambda_5(\Phi_1^\dagger\Phi_2)^2 + [\lambda_6\Phi_1^\dagger\Phi_1 \right. \\ & \left. + \lambda_7\Phi_2^\dagger\Phi_2]\Phi_1^\dagger\Phi_2 + \text{H.c.}\right\}. \end{aligned} \quad (4)$$

Imposing the global U(1) symmetry eliminates m_{12}^2, λ_5, λ_6, and λ_7. The global U(1) symmetry is broken explicitly by reintroducing a small value for m_{12}^2. This leaves the Higgs potential [5],[3]

[2]While we have not made a detailed study of charged Higgs detection prospects at 7 TeV pp center-of-mass energy, we note that the cross section for the most dangerous WW background is about 2.5 times smaller at 7 TeV. However, the signal cross section is also about 2.5 (4.5) times smaller at this energy for $M_{H^+} = 100$ (300) GeV. Furthermore, the LHC is anticipated to collect only about 1 fb^{-1} of integrated luminosity at 7 TeV. We thus expect detection or even exclusion of the process considered here to be unfeasible in the current 7 TeV LHC run.

[3]Note that using a Z_2 symmetry instead of the global U(1) would allow a nonzero λ_5 term.

$$V = m_{11}^2\Phi_1^\dagger\Phi_1 + m_{22}^2\Phi_2^\dagger\Phi_2 - [m_{12}^2\Phi_1^\dagger\Phi_2 + \text{H.c.}] + \frac{1}{2}\lambda_1(\Phi_1^\dagger\Phi_1)^2 + \frac{1}{2}\lambda_2(\Phi_2^\dagger\Phi_2)^2 + \lambda_3(\Phi_1^\dagger\Phi_1)(\Phi_2^\dagger\Phi_2) + \lambda_4(\Phi_1^\dagger\Phi_2)(\Phi_2^\dagger\Phi_1). \quad (5)$$

Stability of the potential at large field values requires λ_1, $\lambda_2 > 0$, $\lambda_3 > -\sqrt{\lambda_1\lambda_2}$, and $\lambda_4 > -\sqrt{\lambda_1\lambda_2} - \lambda_3$. We want v_1 to arise through the usual spontaneous symmetry breaking mechanism, which is achieved when $m_{11}^2 < 0$. We do not want the global U(1) to also be broken spontaneously, as that will create a very light pseudo-Nambu-Goldstone boson, which is incompatible with standard big-bang nucleosynthesis; thus we require that the curvature of the potential in the v_2 direction at zero Φ_2 field value be positive, i.e., $m_{22}^2 + (\lambda_3 + \lambda_4)v_1^2/2 > 0$.

To find the values of the vevs in terms of the parameters of the Higgs potential, we apply the minimization conditions,

$$\left.\frac{\partial V}{\partial|\Phi_1|}\right|_{\text{min}} = m_{11}^2 v_1 - m_{12}^2 v_2 + \frac{1}{2}\lambda_1 v_1^3 + \frac{1}{2}(\lambda_3 + \lambda_4)v_1 v_2^2 = 0$$
$$\left.\frac{\partial V}{\partial|\Phi_2|}\right|_{\text{min}} = m_{22}^2 v_2 - m_{12}^2 v_1 + \frac{1}{2}\lambda_2 v_2^3 + \frac{1}{2}(\lambda_3 + \lambda_4)v_1^2 v_2 = 0. \quad (6)$$

Since we will require $m_{12}^2 \ll v_1^2$, we can ignore m_{12}^2 and v_2 when finding the value of v_1. This yields

$$v_1^2 = \frac{-2m_{11}^2}{\lambda_1}. \quad (7)$$

For v_2, we need to consider m_{12}^2, although again we may ignore higher order terms in m_{12}^2/v_1^2; this yields

$$v_2 = \frac{m_{12}^2 v_1}{m_{22}^2 + \frac{1}{2}(\lambda_3 + \lambda_4)v_1^2}. \quad (8)$$

We will choose parameters so that $v_1 \simeq 246$ GeV and $v_2 \sim$ eV. This requires $m_{12}^2 \sim (\text{MeV})^2$. We note that because m_{12}^2 is the only source of breaking of the global U(1) symmetry, its size is technically natural; i.e., radiative corrections to m_{12}^2 are proportional to m_{12}^2 itself and are only logarithmically sensitive to the high-scale cutoff [5].

The mass eigenstates of the charged and CP-odd neutral scalars are given by

$$G^+ = \phi_1^+ \sin\beta + \phi_2^+ \cos\beta \simeq \phi_1^+$$
$$H^+ = \phi_1^+ \cos\beta - \phi_2^+ \sin\beta \simeq -\phi_2^+.$$
$$G^0 = \phi_1^{0,i} \sin\beta + \phi_2^{0,i} \cos\beta \simeq \phi_1^{0,i} \quad (9)$$
$$A^0 = \phi_1^{0,i} \cos\beta - \phi_2^{0,i} \sin\beta \simeq -\phi_2^{0,i}$$

where we define $\tan\beta \equiv v_1/v_2 \sim 10^{11}$. G^+ and G^0 are the Goldstone bosons, which do not appear as physical particles in the unitarity gauge. H^+ and A^0 are the physical charged and CP-odd neutral Higgs states and are almost entirely contained in Φ_2. Neglecting contributions of order m_{12}^2 and v_2^2, the masses of H^+ and A^0 are [5]

$$M_{H^+}^2 = m_{22}^2 + \frac{1}{2}\lambda_3 v_1^2$$
$$M_A^2 = m_{22}^2 + \frac{1}{2}(\lambda_3 + \lambda_4)v_1^2 = M_{H^+}^2 + \frac{1}{2}\lambda_4 v_1^2. \quad (10)$$

The mass matrix for the CP-even neutral states is almost diagonal, yielding only very tiny mixing of order v_2/v_1. Ignoring the mixing, the eigenstates are $h^0 \simeq \phi_1^{0,r}$ (SM-like) and $H^0 \sim \phi_2^{0,r}$, with masses [5]

$$M_h^2 = m_{11}^2 + \frac{3}{2}\lambda_1 v_1^2 = \lambda_1 v_1^2$$
$$M_H^2 = m_{22}^2 + \frac{1}{2}(\lambda_3 + \lambda_4)v_1^2 = M_A^2. \quad (11)$$

After diagonalizing the neutrino mass matrix, Eq. (3) yields the following couplings to the new physical Higgs states:

$$\mathcal{L}_{\text{Yuk}} \supset -\frac{m_{\nu_i}}{v_2}H^0\bar{\nu}_i\nu_i + i\frac{m_{\nu_i}}{v_2}A^0\bar{\nu}_i\gamma_5\nu_i - \frac{\sqrt{2}m_{\nu_i}}{v_2}[U_{\ell i}^* H^+\bar{\nu}_i P_L e_\ell + \text{H.c.}], \quad (12)$$

where $U_{\ell i}$ is the Pontecorvo-Maki-Nakagawa-Sakata (PMNS) matrix, defined according to $\nu_\ell = \sum_i U_{\ell i}\nu_i$, where ν_ℓ are the neutrino flavor eigenstates.

The PMNS matrix can be parameterized in terms of three mixing angles θ_{ij} (with $ij = 12$, 23, and 13) and a phase δ according to (see, e.g., Ref. [12]),

$$U_{\ell i} = \begin{pmatrix} c_{12}c_{13} & s_{12}c_{13} & s_{13}e^{-i\delta} \\ -s_{12}c_{23} - c_{12}s_{23}s_{13}e^{i\delta} & c_{12}c_{23} - s_{12}s_{23}s_{13}e^{i\delta} & s_{23}c_{13} \\ s_{12}s_{23} - c_{12}c_{23}s_{13}e^{i\delta} & -c_{12}s_{23} - s_{12}c_{23}s_{13}e^{i\delta} & c_{23}c_{13} \end{pmatrix}, \quad (13)$$

where $c_{ij} \equiv \cos\theta_{ij}$ and $s_{ij} \equiv \sin\theta_{ij}$. The 2σ experimentally-allowed ranges for the three mixing angles and the neutrino mass-squared differences are given in Table I. The phase δ and the mass of the lightest neutrino are undetermined, although tritium beta decay experiments set an upper limit on the neutrino masses of about 2 eV [13].

Since the decays of H^0 and A^0 to two neutrinos will be invisible to a collider detector, the decay of most interest is

TABLE I. Current values of the neutrino mixing parameters and mass-squared differences, from the global fit to neutrino oscillation data performed in Ref. [12]. Uncertainties quoted are the 2σ ranges. Note that the constraint on $\sin\theta_{13}$ is only an upper bound, and that the sign of ΔM^2 is not yet known.

Parameter	Value
$\sin^2\theta_{12}$	$0.314(1^{+0.18}_{-0.15})$
$\sin^2\theta_{23}$	$0.44(1^{+0.41}_{-0.22})$
$\sin^2\theta_{13}$	$0.9^{+2.3}_{-0.9}\times 10^{-2}$
$\Delta m^2 \equiv m^2_{\nu_2} - m^2_{\nu_1}$	$7.92(1\pm 0.09)\times 10^{-5}$ eV^2
$\Delta M^2 \equiv m^2_{\nu_3} - \frac{1}{2}(m^2_{\nu_1} + m^2_{\nu_2})$	$\pm 2.4(1^{+0.21}_{-0.26})\times 10^{-3}$ eV^2

$H^+ \to \ell^+\nu$. The charged Higgs can decay into all nine combinations of $\ell_i\nu_j$; summing over neutrino mass eigenstates, the partial width to a particular charged lepton ℓ is [5]

$$\Gamma(H^+ \to \ell^+\nu) = \frac{M_{H^+}\langle m^2_\nu\rangle_\ell}{8\pi v_2^2}, \tag{14}$$

where we define the expectation value of the neutrino mass-squared in a flavor eigenstate by [14]

$$\langle m^2_\nu\rangle_\ell = \sum_i m^2_{\nu_i}|U_{\ell i}|^2. \tag{15}$$

In what follows we work under the assumption that $M_{H^0,A^0} > M_{H^+}$, i.e., $\lambda_4 > 0$, so that the decays $H^+ \to W^+H^0$, W^+A^0 will be kinematically forbidden. The branching ratios of the charged Higgs are then completely determined by the neutrino masses and mixing:

$$\mathrm{BR}\,(H^+ \to \ell^+\nu) = \frac{\langle m^2_\nu\rangle_\ell}{\sum_\ell\langle m^2_\nu\rangle_\ell} = \frac{\langle m^2_\nu\rangle_\ell}{\sum_i m^2_{\nu_i}}, \tag{16}$$

where we used the unitarity of the PMNS matrix to simplify the denominator.

The sign of the larger neutrino mass splitting ΔM^2 is unknown (see Table I). The situation in which ΔM^2 is positive, so that ν_3 is the heaviest neutrino, is called the normal neutrino mass hierarchy, while the situation in which ΔM^2 is negative, so that ν_1 and ν_2 are heavier, is called the inverted hierarchy. We compute the charged Higgs branching fractions as a function of the lightest neutrino mass for both hierarchies, scanning over the 2σ allowed ranges of the neutrino parameters as given in Table I. Results are shown in Fig. 1.[4] The large spread in the branching ratios to $\mu\nu$ and $\tau\nu$ for lightest neutrino masses below about 0.06 eV is due to the current experimental uncertainty in $\sin^2\theta_{23}$, which controls the relative amount of ν_μ and ν_τ in the isolated mass eigenstate ν_3.

Limits on the model parameters were discussed in Ref. [5]. The most significant for our purposes is from searches for leptons plus missing energy at the CERN Large Electron-Positron Collider, which put a lower bound on the charged Higgs mass of 65–85 GeV, depending on the mass of the lightest neutrino. Big-bang nucleosynthesis also puts an upper bound on the neutrino Yukawa couplings of

$$y^\nu_i \equiv \frac{\sqrt{2}m_{\nu_i}}{v_2} \lesssim \frac{1}{30}\left[\frac{M_{H^+}}{100\ \mathrm{GeV}}\right]\left[\frac{1/\sqrt{2}}{|U_{\ell i}|}\right]. \tag{17}$$

III. SIGNAL AND BACKGROUND AT THE LHC

In most other two-Higgs-doublet models, the charged Higgs decay rate to a particular charged lepton is proportional to the square of the charged lepton mass (see, e.g., Ref. [11]). Such a charged Higgs therefore decays predominantly to $\tau\nu$, with decays to $\mu\nu$, $e\nu$ below 1%. In our neutrino-mass model, however, the charged Higgs decay rate to a particular charged lepton is instead proportional to the square of the mass of the corresponding neutrino flavor eigenstate. As a result, the branching fraction to $e\nu$ and/or $\mu\nu$ will always be sizable. In particular, in the normal hierarchy $\mathrm{BR}(H^+ \to \mu\nu) \simeq 1/2$, in the inverted hierarchy $\mathrm{BR}(H^+ \to e\nu) \simeq 1/2$ and $\mathrm{BR}(H^+ \to \mu\nu) \simeq 1/4$, and for a degenerate neutrino spectrum $\mathrm{BR}(H^+ \to e\nu) \simeq \mathrm{BR}(H^+ \to \mu\nu) \simeq 1/3$, as shown in Fig. 1. Considering the high detection efficiency and lower fake rates of e and μ compared to τ, we study H^+H^- pair production at the LHC mediated by a photon or Z, followed by decays to e or μ with missing transverse momentum. We consider two scenarios, $M_{H^+} = 100$ and 300 GeV, and present results as a function of the lightest neutrino mass for both the normal and inverted hierarchy.

The process of interest is $pp \to H^+H^- \to \ell\ell'\bar\nu_\ell\nu_{\ell'}$, with $\ell\ell' = e^+e^-$, $\mu^+\mu^-$, and $e^\pm\mu^\mp$. The relevant backgrounds are $pp \to VV \to \ell\ell'\bar\nu\nu$ with $VV = W^+W^-$, ZZ, or $Z\gamma$ and the neutrinos of any type, and $pp \to t\bar t \to \ell\ell'\bar\nu_\ell\nu_{\ell'}b\bar b$. In spite of the presence of the extra b jets that can be vetoed, the $t\bar t$ process is important because of its exceptionally high cross section at the LHC.

A. Event generation

We simulated the signal and background processes with the parton-level Monte Carlo MADGRAPH/MADEVENT version 4 [8]. We present both a parton-level analysis and an analysis including showering, hadronization, and a fast detector simulation using a PYTHIA-PGS package designed to be used with MADEVENT. PYTHIA (version 6.4.20) [9] generates initial- and final-state radiation and hadronizes the final-state quarks and gluons, while PGS (Pretty Good Simulation of High Energy Collisions, version 4) [10] is a

[4]We disagree with the charged Higgs branching fractions to leptons presented in Ref. [4] for the Z_2 model of Ref. [2]; these decays should have the same relative branching fractions as in our model.

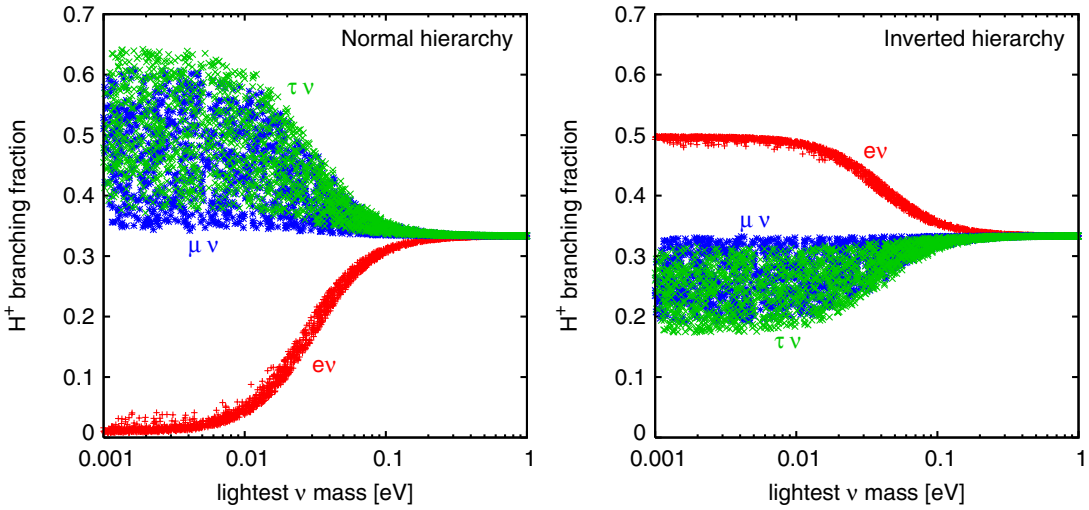

FIG. 1 (color online). Charged Higgs decay branching fractions to $e\nu$, $\mu\nu$, and $\tau\nu$ as a function of the lightest neutrino mass.

basic detector simulator—we used the default settings for ATLAS. For the signal process we generated 10 000 unweighted events in each of the e^+e^-, $\mu^+\mu^-$, and μ^+e^- final states. For both the VV and $t\bar{t}$ backgrounds we generated 100 000 unweighted events in each of the three leptonic final states. We incorporated the μ^-e^+ final state by doubling the μ^+e^- cross sections. For the backgrounds we used the default SM branching fractions from MADGRAPH/MADEVENT, given in Table II.

Although MADGRAPH/MADEVENT is a tree-level event generator, we partially incorporated next-to-leading-order (NLO) QCD corrections. We did this for two reasons. First, QCD corrections have a significant effect on the signal and background (especially $t\bar{t}$) cross sections, as well as significantly reducing the QCD scale uncertainty, so that using NLO cross sections lets us obtain more reliable results. Second, for the $M_{H^+} = 100$ GeV simulation we will apply a jet veto to reduce the $t\bar{t}$ background, which will also affect the signal and VV background once initial-state radiation is included. While this could be simulated by running the no-jet events through PYTHIA, a parton-level simulation of the H^+H^-j and VVj processes provides a more accurate description of jet kinematics. Because these one-jet processes make up part of the NLO QCD cross section for the corresponding no-jet processes, we must incorporate the NLO cross sections for consistency, as follows.

TABLE II. Default SM branching fractions used in MADGRAPH/MADEVENT [8].

Process	Branching fraction
$W^+ \to \ell^+\nu_\ell$ ($\ell = e$ or μ)	0.1068
$Z \to \ell^+\ell^-$ ($\ell = e$ or μ)	0.0336
$Z \to \nu\bar{\nu}$ (all 3 neutrinos)	0.2000
$t \to W^+b$	1.0000

In the absence of a full NLO Monte Carlo, NLO QCD corrections are usually incorporated by multiplying the leading-order (LO) cross section—and the cross section corresponding to each simulated event both before and after cuts—by a k-factor equal to the ratio of the NLO cross section to the tree-level cross section. In our case, however, our jet veto will affect LO events (which have no jet) and NLO events (which can have a final-state jet) differently. We deal with this by simulating $pp \to H^+H^-j$ and $pp \to VVj$ with the same decay final states as considered in the no-jet processes. For simplicity we generate the same number of events with an additional jet at the parton level as were generated for the no-jet processes. Because the $t\bar{t}$ background already contains two jets at leading order, we do not separately generate events with additional jets for this background. To avoid the collinear and infrared singularities, we apply a minimum p_T cut of 10 GeV on the jet at the event-generation level.

The square of the NLO matrix element can be expressed up to order α_s as

$$|\mathcal{M}|^2_{\rm NLO} = |\mathcal{M}_{\rm LO} + \mathcal{M}_{1\,\rm loop}|^2 + |\mathcal{M}|^2_{1\,\rm jet}. \qquad (18)$$

We used MADGRAPH/MADEVENT to calculate the cross sections corresponding to $\mathcal{M}_{\rm LO}$ and $\mathcal{M}_{1\,\rm jet}$. We computed the NLO cross section for $pp \to H^+H^-$ at the LHC using the public FORTRAN code PROSPINO [15,16] with CTEQ6 parton densities [17], with the renormalization and factorization scales set equal to M_{H^+}. We took the NLO cross sections for the SM W^+W^- and ZZ background processes from Ref. [18]. This paper quotes results using both the MRS98 and CTEQ5 parton densities, with results differing by $\sim 6\%$; since we use CTEQ6 for the tree-level MADGRAPH/MADEVENT calculation, we take the results using the CTEQ5 parton densities for consistency. For events with $e^\pm\mu^\mp$ in the final state, only the cross section for

TABLE III. NLO cross sections for signal and background processes (before decays) at the LHC (14 TeV). The $t\bar{t}$ cross section also includes a resummation of next-to-leading logarithmic corrections.

Process	Cross section	Source
$pp \to H^+H^-$ ($M_{H^+} = 100$ GeV)	295 fb	PROSPINO[15,16]
$pp \to H^+H^-$ ($M_{H^+} = 300$ GeV)	5.32 fb	PROSPINO [15,16]
$pp \to W^+W^-$	127.8 pb	Ref. [18]
$pp \to ZZ$	17.2 pb	Ref. [18]
$pp \to t\bar{t}$	833 pb	Ref. [19]

W^+W^- is relevant; for events with $\mu^+\mu^-$ or e^+e^- in the final state, both the W^+W^- and ZZ processes contribute and we add the cross sections at both LO and NLO. We took the $t\bar{t}$ cross section from Ref. [19], which includes both NLO and next-to-leading logarithmic corrections. The remaining scale uncertainty is about $\pm 5\%$ when the factorization and renormalization scales are varied between $m_t/2$ and $2m_t$. The relevant cross sections are given in Table III.

We find that with our generator-level jet p_T cut on $\sigma_{1\,\mathrm{jet}}$, $\sigma_{\mathrm{NLO}} < \sigma_{\mathrm{LO}} + \sigma_{1\,\mathrm{jet}}$, so the one-loop matrix element must interfere destructively with the LO matrix element. Thus the generated cross section from the LO process must be scaled down in order to incorporate the effects of the one-loop correction. For the parton-level simulation, the relevant scale factor is determined by solving for k in the equation,

$$\sigma_{\mathrm{NLO}} = k\sigma_{\mathrm{LO}} + \sigma_{1\,\mathrm{jet}}, \tag{19}$$

before cuts are applied, and then using this equation with the same value of k to calculate the surviving σ_{NLO} after the cuts are applied to the LO and one-jet MADGRAPH/MADEVENT simulated results.

For the PYTHIA-PGS simulation, the simulated events have extra jets produced by PYTHIA and ''measured'' jet p_T smeared by PGS. To avoid double-counting, we use the following equation with two constants:

$$\sigma_{\mathrm{NLO}} = m\sigma^{\mathrm{cut}}_{\mathrm{LO}} + n\sigma^{\mathrm{cut}}_{1\,\mathrm{jet}}, \tag{20}$$

where $\sigma^{\mathrm{cut}}_{\mathrm{LO}}$ and $\sigma^{\mathrm{cut}}_{1\,\mathrm{jet}}$ are the cross sections identified by PGS as having no jets and at least one jet, respectively, with $p_T > 10$ GeV, out of the combined LO and one-jet generated samples. The constants m and n are determined by $m\sigma^{\mathrm{cut}}_{\mathrm{LO}} = k\sigma_{\mathrm{LO}}$ and $n\sigma^{\mathrm{cut}}_{1\,\mathrm{jet}} = \sigma_{1\,\mathrm{jet}}$ using k from Eq. (19). Equation (20) with the same values of m and n is then used after cuts to calculate the surviving σ_{NLO}.

B. Cuts

We apply four cuts to reduce the background, summarized in Table IV. The first cut checks for the presence of two opposite-sign leptons each with $p_T > 20$ GeV and missing transverse momentum of at least 30 GeV. For the parton-level simulation, we also apply acceptance cuts on the pseudorapidity of both leptons, $|\eta| < 3.0$ for electrons and $|\eta| < 2.4$ for muons. Second, for the e^+e^- and $\mu^+\mu^-$ final states we veto events for which the dilepton invariant mass falls between 80 and 100 GeV, in order to eliminate background from $Z(\to \ell\ell) + p_T^{\mathrm{miss}}$. This will also eliminate the majority of any background from Z + jets with fake p_T^{miss}, which we did not simulate. The third cut vetoes events containing a jet with $p_T > 30$ GeV; for the parton-level simulation, we require that this jet falls in the rapidity range $|\eta| < 5.0$. This eliminates more than 97% of the $t\bar{t}$ background, but also reduces the signal by about a factor of 2. We find that this cut is useful for $M_{H^+} = 100$ GeV. For $M_{H^+} = 300$ GeV the signal cross section is considerably smaller and the signal events will be better separated from background in our final cut variable, so that we obtain better sensitivity without the jet veto.

TABLE IV. Summary of cuts.

Cut name	Explanation
Basic cuts	Present are a lepton and antilepton, each with $p_T^\ell > 20$ GeV, and missing transverse momentum $p_T^{\mathrm{miss}} > 30$ GeV. For the parton level results, we also apply lepton acceptance cuts of $\lvert\eta_e\rvert < 3.0$ and $\lvert\eta_\mu\rvert < 2.4$.
Z pole veto	To eliminate events that include $Z \to \ell^+\ell^-$, we veto events in which the invariant mass of e^+e^- or $\mu^+\mu^-$ is between 80 and 100 GeV (not applied to the $e^\pm\mu^\mp p_T^{\mathrm{miss}}$ final state).
Jet veto	Designed to reduce $t\bar{t}$ background, any event with a jet with $p_T^{\mathrm{jet}} > 30$ GeV was rejected. For the parton level results, this veto is only applied when $\lvert\eta_{\mathrm{jet}}\rvert < 5.0$. (Applied only for $M_{H^+} = 100$ GeV.)
M_{T2} cut	To reduce the W^+W^- and $t\bar{t}$ backgrounds, we make use of the larger mass of H^+ compared to the intermediate W bosons in both backgrounds by cutting on M_{T2} (defined in Eq. (21)). For $M_{H^+} = 100$ GeV we require $M_W < M_{T2} < 100$ GeV and for $M_{H^+} = 300$ GeV we require 150 GeV $< M_{T2} < 300$ GeV.

The final cut is on the variable M_{T2}, defined as [20]

$$M_{T2}^2 = \min_{q_T^{\mathrm{miss}(1)} + q_T^{\mathrm{miss}(2)} = p_T^{\mathrm{miss}}} [\max\{m_T^2(p_T^{\ell(1)}, q_T^{\mathrm{miss}(1)}), m_T^2(p_T^{\ell(2)}, q_T^{\mathrm{miss}(2)})\}], \tag{21}$$

where m_T^2 is the square of the transverse mass (ignoring the charged lepton and neutrino masses),

$$m_T^2(p_T^\ell, q_T^{\mathrm{miss}}) = 2(|\vec{p}_T^{\,\ell}||\vec{q}_T^{\,\mathrm{miss}}| - \vec{p}_T^{\,\ell} \cdot \vec{q}_T^{\,\mathrm{miss}}). \tag{22}$$

In other words, M_{T2} is determined by making a guess for the transverse momenta of the two neutrinos (constrained by the measured total missing transverse momentum) and computing the transverse masses of the two $\ell\nu$ systems; the guess is then varied until the larger of the two reconstructed transverse masses is minimized.

For equal-mass intermediate particles each decaying to $\ell\nu$, the M_{T2} distribution has an upper endpoint at the mass of the intermediate particle. Thus by cutting out events with $M_{T2} < M_W$, all the W^+W^- background should be eliminated (the endpoint is in fact smeared out by the finite W width and momentum resolution of the detector). Since the leptons and missing transverse momentum in the $t\bar{t}$ process also come from decays of on-shell W^+W^-, this background should be eliminated as well. There is also a small contribution to the VV background from nonresonant processes that can have $M_{T2} > M_W$. Since all signal events will have $M_{T2} < M_{H^+}$, we also cut out events with $M_{T2} > M_{H^+}$ in an effort to reduce the background from these nonresonant VV processes. For $M_{H^+} = 300$ GeV, we find that raising the minimum cut on M_{T2} to 150 GeV reduces the tail of the nonresonant VV events without reducing the signal too much.

In Fig. 2 we show the M_{T2} distributions for signal and background processes in the $e^+e^-p_T^{\mathrm{miss}}$ channel for $M_{H^+} = 100$ and 300 GeV after the other cuts have been applied, for the PYTHIA-PGS simulation. Note that the $t\bar{t}$ background distribution has a maximum M_{T2} value a little above the W mass, so that it can be eliminated with a high enough cut on M_{T2}, as we do for the case of $M_{H^+} = 300$ GeV. (The higher M_{T2} endpoint for $t\bar{t}$ in the right-hand plot in Fig. 2 is due to the absence of the jet veto, resulting in much higher $t\bar{t}$ statistics.) The VV background also falls off dramatically around $M_{T2} \sim M_W$; however, due to nonresonant diagrams without on-shell intermediate W pairs, this background extends to much higher values of M_{T2}. With our simulation statistics, a single $\bar{t}t$ event corresponds to a cross section of about 0.1 fb, while a single VV event corresponds to a cross section of about 0.01 fb.

C. Results

The efficiency of each cut on σ_{NLO} for the $e^+e^-p_T^{\mathrm{miss}}$ final state is displayed in Tables V, VI, and VII. Cut efficiencies for $\mu^+\mu^-p_T^{\mathrm{miss}}$ are displayed in Tables VIII, IX, and X, and for $e^\pm\mu^\mp p_T^{\mathrm{miss}}$ in Tables XI, XII, and XIII. We give efficiencies for both the parton-level simulation

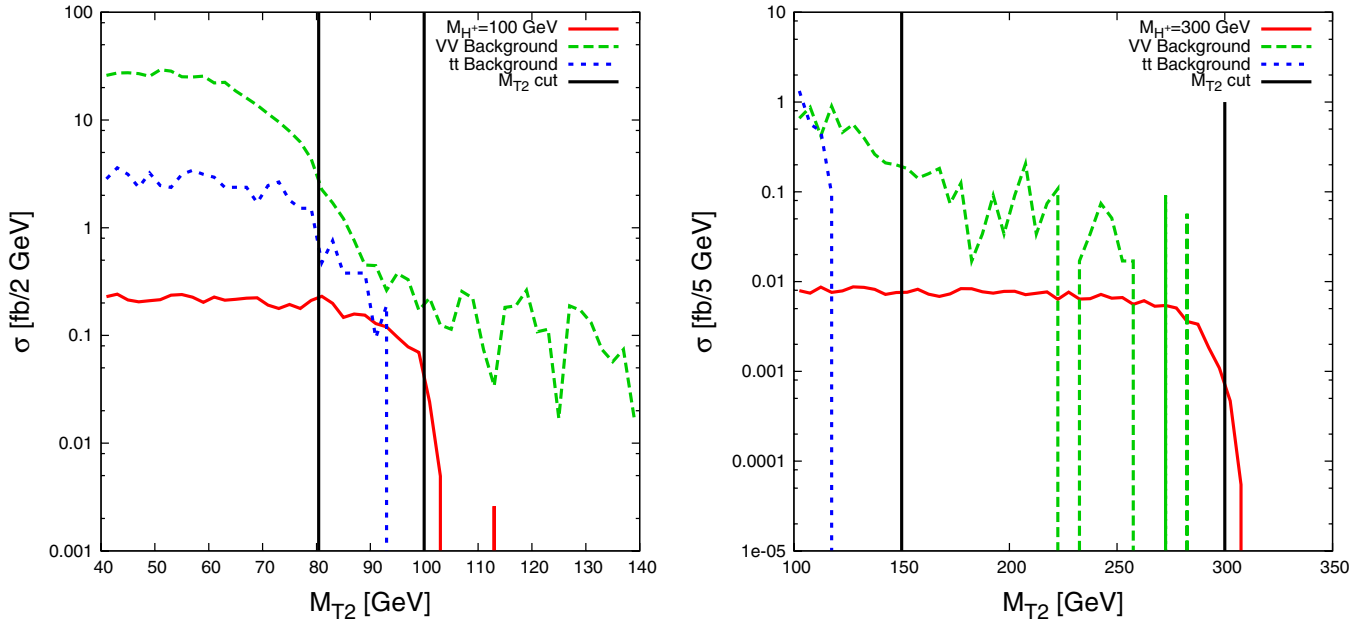

FIG. 2 (color online). M_{T2} distributions after other cuts have been applied for the $e^+e^-p_T^{\mathrm{miss}}$ final state, with $M_{H^+} = 100$ GeV (left, with jet veto) and 300 GeV (right, no jet veto). For the signal we take $\mathrm{BR}(H^+ \to e^+\nu) = 1/3$, which occurs for a degenerate neutrino spectrum. The M_{T2} cut window is shown by the vertical lines.

TABLE V. Cut efficiencies for the signal process $pp \to e^+e^- p_T^{\rm miss}$ via H^+H^-. The efficiency of each cut is defined as the cross section that passed the cut divided by the cross section that passed the previous cut. The cumulative efficiency is the cross section that passed all the cuts divided by the original cross section. The jet veto is not applied for $M_{H^+} = 300$ GeV. The M_{T2} cut is $M_W < M_{T2} < 100$ GeV for $M_{H^+} = 100$ GeV, and 150 GeV $< M_{T2} < 300$ GeV for $M_{H^+} = 300$ GeV.

	$M_{H^+} = 100$ GeV		$M_{H^+} = 300$ GeV	
Cuts	Parton	PYTHIA/PGS	Parton	PYTHIA/PGS
Basic cuts	0.626 44	0.478 60	0.929 61	0.721 05
Z pole veto	0.907 54	0.901 65	0.977 32	0.977 24
Jet veto	0.684 33	0.607 17	···	···
M_{T2} cut	0.170 75	0.155 42	0.473 17	0.459 45
Cumulative	0.066 43	0.040 72	0.429 88	0.323 75

TABLE VI. As in Table V but for background for $pp \to e^+e^- p_T^{\rm miss}$, with cuts for $M_{H^+} = 100$ GeV.

	VV Background		$t\bar{t}$ Background	
Cuts	Parton	PYTHIA/PGS	Parton	PYTHIA/PGS
Basic cuts	0.427 08	0.339 12	0.584 07	0.406 12
Z pole veto	0.747 27	0.732 55	0.862 36	0.855 01
Jet veto	0.633 06	0.672 99	0.013 18	0.028 56
$M_{W^+} < M_{T2} < 100$ GeV	0.014 01	0.011 47	0.012 05	0.027 16
Cumulative	0.002 83	0.001 92	0.000 08	0.000 27

TABLE VII. As in Table V but for background for $pp \to e^+e^- p_T^{\rm miss}$, with cuts for $M_{H^+} = 300$ GeV.

	VV Background		$t\bar{t}$ Background	
Cuts	Parton	PYTHIA/PGS	Parton	PYTHIA/PGS
Basic cuts	0.427 08	0.339 12	0.584 07	0.406 12
Z pole veto	0.747 27	0.732 55	0.862 36	0.855 01
150 GeV $< M_{T2} < 300$ GeV	0.002 60	0.001 96	0.000 00	0.000 00
Cumulative	0.000 83	0.000 49	0.000 00	0.000 00

TABLE VIII. As in Table V but for the signal process $pp \to \mu^+\mu^- p_T^{\rm miss}$ via H^+H^-.

	$M_{H^+} = 100$ GeV		$M_{H^+} = 300$ GeV	
Cuts	Parton	PYTHIA/PGS	Parton	PYTHIA/PGS
Basic cuts	0.517 13	0.436 80	0.848 10	0.698 45
Z pole veto	0.908 69	0.900 75	0.977 56	0.976 96
Jet veto	0.683 10	0.578 31	···	···
M_{T2} cut	0.168 75	0.173 20	0.478 02	0.468 47
Cumulative	0.054 17	0.039 41	0.396 32	0.319 66

TABLE IX. As in Table V but for background for $pp \to \mu^+\mu^- p_T^{\rm miss}$, with cuts for $M_{H^+} = 100$ GeV.

	VV Background		$t\bar{t}$ Background	
Cuts	Parton	PYTHIA/PGS	Parton	PYTHIA/PGS
Basic cuts	0.329 59	0.282 26	0.525 93	0.390 48
Z pole veto	0.738 39	0.730 98	0.860 21	0.854 89
Jet veto	0.627 03	0.632 04	0.013 46	0.022 82
$M_{W^+} < M_{T2} < 100$ GeV	0.013 24	0.015 54	0.006 57	0.036 75
Cumulative	0.002 02	0.002 03	0.000 04	0.000 28

TABLE X. As in Table V but for background for $pp \to \mu^+\mu^- p_T^{\rm miss}$, with cuts for $M_{H^+} = 300$ GeV.

	VV Background		$t\bar{t}$ Background	
Cuts	Parton	PYTHIA/PGS	Parton	PYTHIA/PGS
Basic cuts	0.329 59	0.282 26	0.525 93	0.390 48
Z pole veto	0.738 39	0.730 98	0.860 21	0.854 89
150 GeV $< M_{T2} < 300$ GeV	0.002 88	0.002 39	0.000 00	0.000 00
Cumulative	0.000 70	0.000 49	0.000 00	0.000 00

TABLE XI. As in Table V but for the signal process $pp \to e^\pm \mu^\mp p_T^{\rm miss}$ via H^+H^-.

	$M_{H^+} = 100$ GeV		$M_{H^+} = 300$ GeV	
Cuts	Parton	PYTHIA/PGS	Parton	PYTHIA/PGS
Basic cuts	0.561 31	0.457 43	0.882 49	0.708 32
Jet veto	0.687 83	0.595 28	...	...
M_{T2} cut	0.168 57	0.161 21	0.474 27	0.463 73
Cumulative	0.065 08	0.043 90	0.418 54	0.328 47

TABLE XII. As in Table V but for background for $pp \to e^\pm \mu^\mp p_T^{\rm miss}$, with cuts for $M_{H^+} = 100$ GeV.

	VV Background		$t\bar{t}$ Background	
Cuts	Parton	PYTHIA/PGS	Parton	PYTHIA/PGS
Basic cuts	0.358 35	0.304 23	0.552 97	0.395 56
Jet veto	0.655 90	0.685 72	0.012 55	0.025 92
$M_{W^+} < M_{T2} < 100$ GeV	0.008 60	0.012 07	0.015 85	0.030 18
Cumulative	0.002 02	0.002 52	0.000 11	0.000 31

TABLE XIII. As in Table V but for background for $pp \to e^\pm \mu^\mp p_T^{\rm miss}$, with cuts for $M_{H^+} = 300$ GeV.

	VV Background		$t\bar{t}$ Background	
Cuts	Parton	PYTHIA/PGS	Parton	PYTHIA/PGS
Basic cuts	0.358 35	0.304 23	0.552 97	0.395 56
150 GeV $< M_{T2} < 300$ GeV	0.000 57	0.000 49	0.000 00	0.000 00
Cumulative	0.000 21	0.000 15	0.000 00	0.000 00

TABLE XIV. Signal over background (S/B) and luminosity required for a 5σ discovery in a single channel for the three signal processes studied, for $M_{H^+} = 100$ and 300 GeV, assuming a degenerate neutrino spectrum so that $\mathrm{BR}(H^+ \to e^+\nu) = \mathrm{BR}(H^+ \to \mu^+\nu) = 1/3$.

M_{H^+}	Channel	S/B	Luminosity for 5σ
100 GeV	$e^+e^- p_T^{\mathrm{miss}}$	0.24	78 fb^{-1}
	$\mu^+\mu^- p_T^{\mathrm{miss}}$	0.22	88 fb^{-1}
	$e^\pm\mu^\mp p_T^{\mathrm{miss}}$	0.22	40 fb^{-1}
300 GeV	$e^+e^- p_T^{\mathrm{miss}}$	0.25	526 fb^{-1}
	$\mu^+\mu^- p_T^{\mathrm{miss}}$	0.25	540 fb^{-1}
	$e^\pm\mu^\mp p_T^{\mathrm{miss}}$	0.89	73 fb^{-1}

and the simulation including showering, hadronization, and fast detector simulation using the PYTHIA-PGS package. All results incorporate NLO corrections as described in Sec. III A.

Consider, for example, the PYTHIA-PGS results in the $e^+e^- p_T^{\mathrm{miss}}$ final state, and assume a degenerate neutrino spectrum so that $\mathrm{BR}(H^+ \to e^+\nu) = 1/3$. In this case, for $M_{H^+} = 100$ GeV, the cuts reduce the charged Higgs signal cross section in this channel from 32.8 fb to 1.34 fb, while reducing the VV background from 1570 fb to 3.01 fb and the $t\bar{t}$ background from 9500 fb to 2.57 fb. The ratio of signal to background cross sections (S/B) is then 0.24. For $M_{H^+} = 300$ GeV, S/B is comparable. These are displayed for all channels for a degenerate neutrino spectrum in Table XIV. In all cases S/B is at least 0.22, comfortably larger than the QCD and parton density uncertainties on the VV and $t\bar{t}$ backgrounds; the overall cross sections of these backgrounds can also be normalized experimentally using M_{T2} regions below M_W.

For $M_{H^+} = 100$ GeV, the background after cuts depends sensitively on the shape of the background M_{T2} distribution just above M_W. This is controlled by the W width and the detector resolution for lepton momenta and missing p_T; its shape should not suffer from QCD or parton-density uncertainties. For $M_{H^+} = 300$ GeV, the shape and normalization of the nonresonant tail of the VV background is especially important. This background is mostly Drell-Yan with an additional on-shell W boson radiated from one of the final-state leptons; the QCD corrections to such processes are well understood. Given enough statistics, the shape of this background could also be normalized using the M_{T2} region above M_{H^+}. Note also that the nonresonant tail of the VV background is significantly smaller for the $e^\pm\mu^\mp$ final state than for the e^+e^- and $\mu^+\mu^-$ final states, leading to a much higher signal purity in this final state for $M_{H^+} = 300$ GeV as shown in the last line of Table XIV (for the lower charged Higgs mass this effect is swamped by the resonant-W contribution).

The integrated luminosity required for a 5σ discovery of H^+H^- is displayed in Fig. 3 for $M_{H^+} = 100$ GeV and Fig. 4 for $M_{H^+} = 300$ GeV, for each channel separately and for all three channels combined. We use the PYTHIA-PGS results and compute only the statistical significance. For the normal hierarchy with $M_{H^+} = 100\,(300)$ GeV, we find 5σ discovery statistics with a minimum of $9\,(56)$ fb^{-1}. For the inverted hierarchy, the minimum

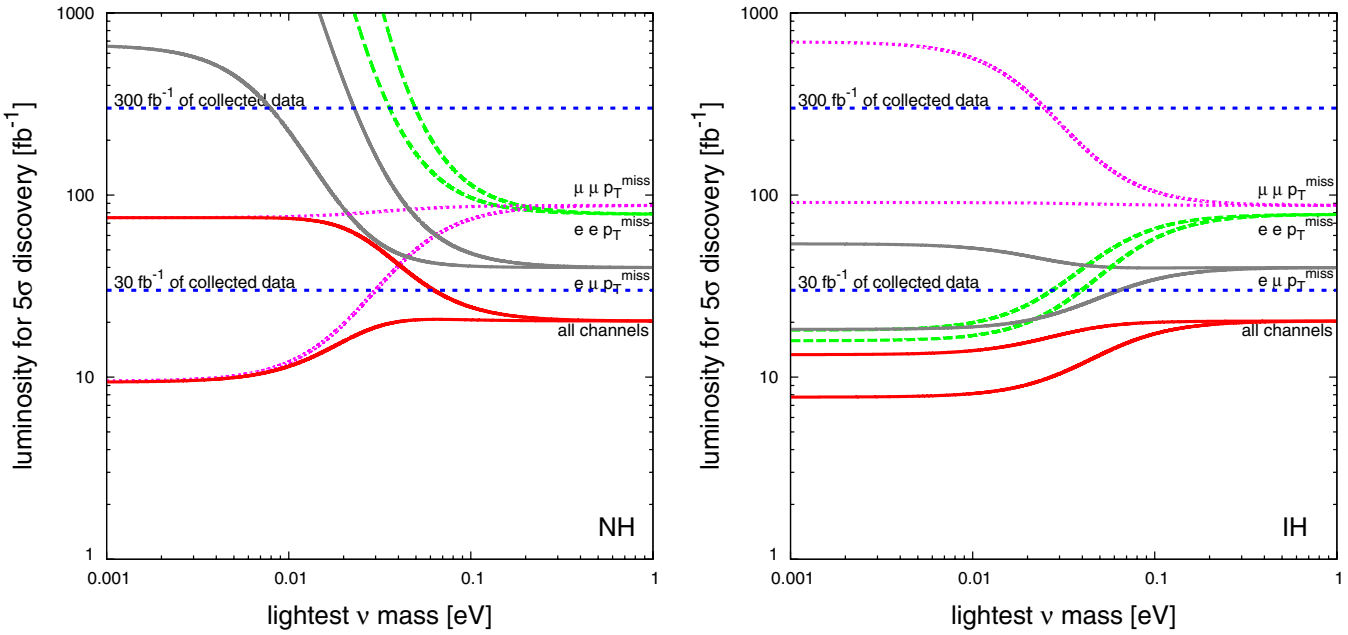

FIG. 3 (color online). Luminosity required at the LHC (14 TeV) for a 5σ discovery if $M_{H^+} = 100$ GeV, for the normal hierarchy (NH, left) and inverted hierarchy (IH, right). The lines for each channel bound the range of required luminosities obtained by scanning over the 2σ allowed ranges of the parameters of the neutrino mixing matrix and mass-squared differences.

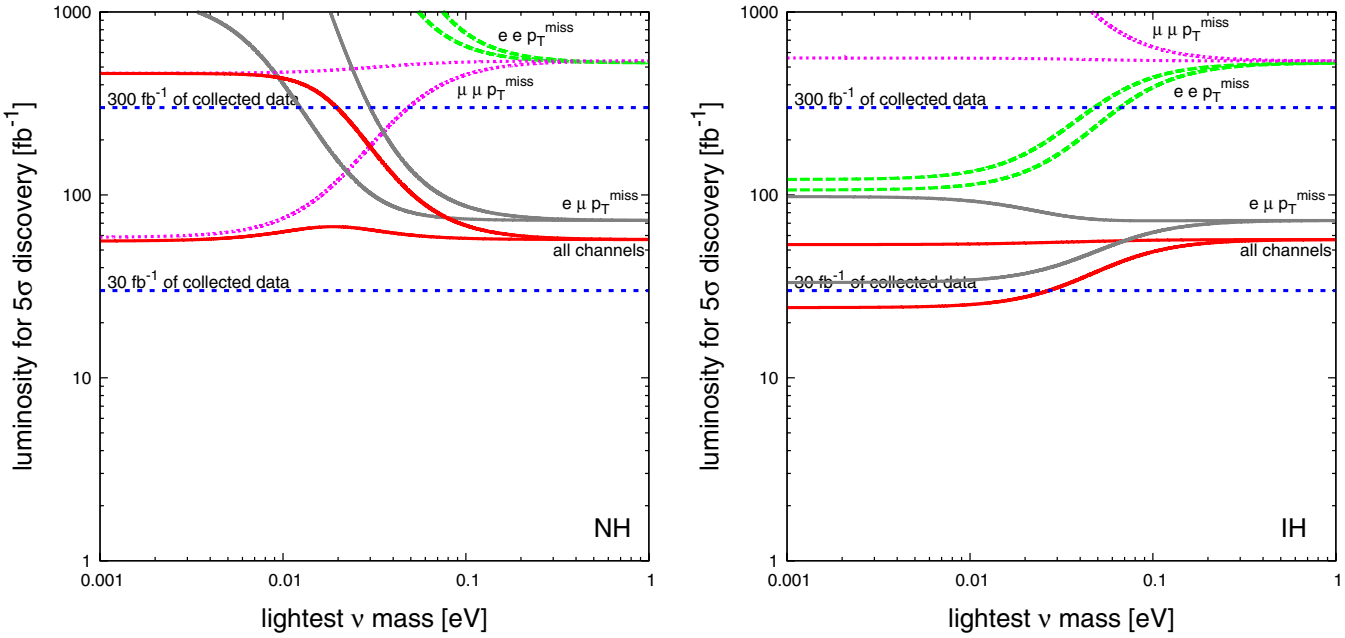

FIG. 4 (color online). As in Fig. 3 but for $M_{H^+} = 300$ GeV.

is 8 (24) fb^{-1}. For the case of degenerate neutrino masses, 20 (57) fb^{-1} is needed. For degenerate neutrino masses, the luminosity needed for a 5σ discovery in each channel separately is given in Table XIV.

IV. DISCUSSION AND CONCLUSIONS

The two-Higgs-doublet model for Dirac neutrino masses studied here provides distinctive leptonic signatures at the LHC due to the characteristic decay pattern of the charged Higgs boson, controlled by the neutrino masses and mixing. We have shown that a simple set of cuts allows discovery of charged Higgs pairs with decays to $\ell\ell^{(\prime)}p_T^{\rm miss}$ with relatively modest integrated luminosity. In particular we found that a cut on the kinematic variable M_{T2} provides very effective suppression of W pair and $t\bar{t}$ backgrounds for charged Higgs masses sufficiently above the W mass.

In the inverted neutrino mass hierarchy, the large branching fractions of the charged Higgs to $e\nu$ and $\mu\nu$ guarantees a 5σ discovery for any allowed neutrino mass and mixing parameter values with only 20 (57) fb^{-1} for $M_{H^+} = 100\,(300)$ GeV. The discovery potential remains remarkably good at $M_{H^+} = 300$ GeV despite the rapidly falling charged Higgs pair production cross section because of the increasing separation of the signal M_{T2} distribution from the background.

In the normal neutrino mass hierarchy, the large uncertainty on the neutrino mixing angle θ_{23} leads to parameter regions in which the charged Higgs decays predominantly to $\tau\nu$, with a branching fraction to light leptons below 40%, resulting in poor discovery sensitivity in the light lepton channels studied in this paper. Away from these parameter regions, the discovery prospects are only slightly worse than in the inverted hierarchy.

As more stringent experimental limits are placed on the neutrino parameters from neutrino oscillation experiments and direct searches for the kinematic neutrino mass in beta decay, the predictions for the charged Higgs branching ratios in this model will tighten. For example, one goal of the currently-running T2K long-baseline neutrino oscillation experiment in Japan is to improve the measurement accuracy of $\sin^2(2\theta_{23})$ by an order of magnitude [21], which would reduce the 2σ spread in the charged Higgs branching ratios to $\mu\nu$ and $\tau\nu$ at low lightest-neutrino mass from the current $\pm 30\%$ to about $\pm 10\%$. Sensitivity to the neutrino mass hierarchy relies on detection of a nonzero θ_{13}, a major goal of T2K and the longer-baseline U.S.-based experiment NOνA currently under construction [22]. The ratios of the signal rates in the three channels considered here would allow the normal, inverted, and degenerate neutrino spectra to be differentiated, providing a key test of the connection of the model to the neutrino sector.

Measurement of the charged Higgs branching fractions will also provide some sensitivity to the mass of the lightest neutrino. For a lightest neutrino mass between about 0.01 and 0.1 eV, the charged Higgs branching ratios vary dramatically with the value of the lightest neutrino mass (Fig. 1); once the measurement of θ_{23} from neutrino oscillations has improved, measurement of the ratio of the $e\nu$ and $\mu\nu$ modes will provide sensitivity to the lightest neutrino mass in this range. This is nicely complementary to the prospects for direct kinematic neutrino mass determination from the Karlsruhe tritium beta decay experiment KATRIN, which is designed to be sensitive down to

neutrino masses of about 0.2 eV [23]—i.e., at the lower end of the degenerate part of the spectrum—and is scheduled to begin commissioning in 2012 [24]. We note that, because the neutrinos in this model are Dirac particles, neutrinoless double beta decay experiments will have no signal and will thus not be sensitive to the neutrino mass scale.

The mass of the charged Higgs is also accessible at the LHC through the signal event kinematics. In particular, the signal M_{T2} distribution is flat up to an endpoint at the charged Higgs mass, as shown in Fig. 2. A fit to this distribution on top of the background should provide a measurement of the charged Higgs mass. This would allow a valuable cross-check of the charged Higgs pair production cross section together with the visible branching fractions as predicted by the neutrino parameters. The pair production cross section is sensitive to the isospin of the charged Higgs through its coupling to the Z boson, allowing the two-doublet nature of the model to be established [5].

We finally comment on the applicability of our results to two other neutrino mass models that contain a charged Higgs boson. First, the Z_2 model of Ref. [2] contains a charged Higgs with partial widths to leptons and LHC production cross section identical to those in our model. The charged Higgs in the Z_2 model differs from ours in that it can also decay to $W^+\sigma$, where the neutral scalar σ is extremely light due to the spontaneous breaking of the Z_2 symmetry. This competing mode dominates unless H^+ is not much heavier than M_W and the neutrino Yukawa couplings are $\mathcal{O}(1)$ [4] (this parameter region is forbidden by standard big-bang nucleosynthesis, but the Z_2 model already requires nonstandard cosmology due to the very light scalar σ). For this parameter range, then, our results should carry over directly. For smaller Yukawa couplings or a heavier H^+, the decays to leptons used in our analysis are suppressed, resulting in a smaller signal on top of the same background.

Second, neutrino masses of Majorana type can be generated by the so-called Type II seesaw mechanism [25], in which an SU(2)-triplet Higgs field $X \equiv (\chi^{++}, \chi^+, \chi^0)^T$ with very small vev is coupled to a pair of SM lepton doublets. LHC phenomenology for this Higgs-triplet model was studied in Ref. [26], which considered signatures from $\chi^{++}\chi^{--}$ and $\chi^{++}\chi^-$ (and the conjugate process) at the LHC. While the decay branching fractions of χ^+ in this model are identical to those of the charged Higgs in our Higgs-doublet model, the LHC production cross section for $\chi^+\chi^-$ in the triplet model is about 2.7 times smaller than for H^+H^- in the doublet model [5], due to the different isospin of χ^+ which modifies its coupling to the Z boson. The signals studied here would thus have a S/B of less than 10% for most channels, potentially leading to problems with background systematics. For sufficiently high charged Higgs mass, though, the $\mu^\pm e^\mp$ channel would still have a decent S/B (33% for $M_{H^+} = 300$ GeV and a degenerate neutrino spectrum); the reduced cross section in the triplet model would however require an integrated luminosity close to 300 fb^{-1} for discovery. In any case, searches for the doubly-charged scalar would yield an earlier discovery of the triplet model.

ACKNOWLEDGMENTS

This work was supported by the Natural Sciences and Engineering Research Council of Canada.

[1] E. Ma, Phys. Rev. Lett. **86**, 2502 (2001).
[2] F. Wang, W. Wang, and J. M. Yang, Europhys. Lett. **76**, 388 (2006); S. Gabriel and S. Nandi, Phys. Lett. B **655**, 141 (2007).
[3] P. Fayet, Nucl. Phys. **B78**, 14 (1974); A. Barroso and J. P. Silva, Phys. Rev. D **50**, 4581 (1994).
[4] S. Gabriel, B. Mukhopadhyaya, S. Nandi, and S. K. Rai, Phys. Lett. B **669**, 180 (2008).
[5] S. M. Davidson and H. E. Logan, Phys. Rev. D **80**, 095008 (2009).
[6] M. Hashimoto and S. Kanemura, Phys. Rev. D **70**, 055006 (2004); **70**, 119901(E) (2004).
[7] G. Marshall, M. McCaskey, and M. Sher, Phys. Rev. D **81**, 053006 (2010).
[8] J. Alwall *et al.*, J. High Energy Phys. 09 (2007) 028.
[9] T. Sjostrand, S. Mrenna, and P. Z. Skands, J. High Energy Phys. 05 (2006) 026.
[10] J. Conway *et al.*, available from http://www.physics.ucdavis.edu/~conway/research/software/pgs/pgs4-general.htm.
[11] J. F. Gunion, H. E. Haber, G. L. Kane, and S. Dawson, *The Higgs Hunter's Guide* (Westview Press, Boulder, Colorado, 2000).
[12] G. L. Fogli, E. Lisi, A. Marrone, and A. Palazzo, Prog. Part. Nucl. Phys. **57**, 742 (2006).
[13] C. Amsler *et al.* (Particle Data Group), Phys. Lett. B **667**, 1 (2008).
[14] T. Fukuyama and K. Tsumura, arXiv:0809.5221.
[15] W. Beenakker, M. Klasen, M. Kramer, T. Plehn, M. Spira, and P. M. Zerwas, Phys. Rev. Lett. **83**, 3780 (1999); **100**, 029901(E) (2008).
[16] A. Alves and T. Plehn, Phys. Rev. D **71**, 115014 (2005).
[17] J. Pumplin, D. R. Stump, J. Huston, H. L. Lai, P. M. Nadolsky, and W. K. Tung, J. High Energy Phys. 07 (2002) 012.
[18] J. M. Campbell and R. K. Ellis, Phys. Rev. D **60**, 113006 (1999).
[19] R. Bonciani, S. Catani, M. L. Mangano, and P. Nason, Nucl. Phys. **B529**, 424 (1998); **B803**, 234(E) (2008).

[20] C. G. Lester and D. J. Summers, Phys. Lett. B **463**, 99 (1999).
[21] M. Zito (T2K Collaboration), J. Phys. Conf. Ser. **110**, 082023 (2008).
[22] NOvA Collaboration, Technical Design Report, http://www-nova.fnal.gov/nova_cd2_review/tdr_oct_23/tdr.htm.
[23] K. Valerius, (KATRIN Collaboration), Proc. Sci., HEP2005 (2006) 166.
[24] T. Thummler, in XXIV International Conference on Neutrino Physics and Astrophysics, Athens, 14–19 June 2010, slides available from http://indico.cern.ch/conferenceDisplay.py?confId=73981.
[25] G. Lazarides, Q. Shafi, and C. Wetterich, Nucl. Phys. **B181**, 287 (1981); J. Schechter and J. W. F. Valle, Phys. Rev. D **22**, 2227 (1980); R. N. Mohapatra and G. Senjanovic, Phys. Rev. D **23**, 165 (1981).
[26] P. Fileviez Perez, T. Han, G. Y. Huang, T. Li, and K. Wang, Phys. Rev. D **78**, 071301 (2008); **78**, 015018 (2008); A. G. Akeroyd, C. W. Chiang, and N. Gaur, J. High Energy Phys. 11 (2010) 005.